Pool Boiling from a Surface with a Porous Layer

Boiling heat transfer from a porous layer sintered on a horizontal heater surface and heated from the base was analyzed for laminar to turbulent regions. The effects of the thickness of the porous layer, particle diameter, porosity, pore size distribution, and the properties of fluids on boiling heat transfer were analyzed. Reynolds number, parameter ψ, and a dimensionless heat flux were related to each other. Most experimental data used in this work fall in the region where the vapor Reynolds number is less than 100; very few data exceeded far beyond 1,000.

For thick porous beds, the thickness no longer affects the heat transfer. For thin porous beds, heat transfer is affected by the thickness of the porous layer. The prediction equations of various investigators for dryout heat flux were put into dimensionless forms and the differences that exist among the equations are explained.

S. M. Lu, R. H. Chang
Chemical Engineering Department
National Taiwan University
Taipei, Taiwan, Republic of China

Introduction

A boiling heat transfer coefficient is known to depend strongly on the characteristics of a heater surface. Heat transfer is enhanced when the surface is not smooth. Different methods have been used to manufacture nonsmooth heat transfer surfaces, and various high-efficiency heating surfaces are available commercially; one type is a surface deposited with a porous matrix. Boiling heat transfer with such a surface has been the interest of many investigators from different fields. The characteristics of the porous matrix used for boiling studies depend on the purpose of the investigation.

For research in the field of heat transfer enhancement, the porous layer may be a thin layer of porous coating, layers of wire meshes, or a thin layer of small metallic granules sintered on the heater surface. A heating surface sintered with granules of high thermal conductivity is characterized by its high heat transfer coefficient and lasting enhancement in heat transfer. In this branch of study, heating is from the base of the porous bed. In the past decade, researches in boiling from such surfaces have accumulated. Enhancement in heat transfer is marked by the shift of the boiling curve leftward when compared with that of a smooth surface. Milton and Gottzmann (1972), Czikk et al. (1981), Ito et al. (1982), and others studied the effects of different porous layers on the boiling curves. However, the relationship between the enhancement and the characteristics of the porous layers has not been well understood.

For research in the field of nuclear reactor safety, the boiling heat transfer in a bed of fuel debris is important to the safety of a reactor. Since the debris generates heat, the heating mode is volumetric; however, both bottom and volumetric heatings have been studied. In many experimental investigations, porous beds were constructed of metallic or nonmetallic granules. The particles composing the beds may not be uniform in size. Particles may be spherical, roughly spherical, or solid granules. The piled granules may either be confined between the base and a porous plate at the top, or merely piled up. In the latter case, when the bed is shallow the particles may be fluidized, and when the bed is thick the lower part of the bed may be considered as a fixed bed, while channeling may occur in the upper part of the bed.

Boiling with a porous layer is a problem of two-phase flow with heat and mass transfer in a porous matrix. The vapor phase flows upward and the liquid phase flows downward to make up for the evaporated liquid. When the liquid supply is insufficient, dryout of the matrix occurs. Exact description of the boiling phenomena in the porous matrix is difficult. However, a phenomenological approach may be used. Several models have been proposed for beds of small and large particles.

For beds of small particles, flow is likely to be laminar. Darcy's equation has been applied to analyze the problem. Bau and Torrance (1982) analyzed the problem without capillary pressure effect. The dryout heat flux was found to be independent of

Correspondence concerning this paper should be addressed to S. M. Lu.

bed height and the two-phase zone was almost isothermal. Udell (1985) also analyzed the one-dimensional problem for the laminar flow case. Capillary pressure gradient was considered. For the case of bottom heating, the dryout heat flux was found to depend on the ratio of kinematic viscosity of liquid to vapor. Jones et al. (1984) proposed a semiempirical equation for the dryout heat flux of laminar and bottom-heating case. Their dryout heat flux is smaller than that found by Bau and Torrance and by Udell. Hardee and Nilson (1977) and Dhir and Catton (1982) analyzed the laminar problem for the volumetric heating case. Their equations for dryout heat flux are about twice greater than that for the bottom-heating case. All these prediction equations, however, have a slope of 2 on a log-log plot of dryout heat flux vs. particle diameter.

For beds of large particles, turbulence is induced. Lipinski (1980) analyzed the problem for the volumetric heating case. Squarer (1981) presented an equation that predicts lower dryout heat flux than that found by Lipinski. Ostensen and Lipinski (1981) and Dhir and Catton (1982) used the flooding model to obtain equations for dryout heat flux. All these prediction equations predict different values for the dryout heat flux but have a slope of 1/2 on a log-log plot of dryout heat flux vs. particle diameter.

There are many practical situations in which the fluid flows are neither laminar nor turbulent. This transition region has been studied by a few investigators. Lipinski (1980) extended Hardee and Nilson's approach to cover both laminar and turbulent regions. His results show agreement with Ostensen in the large-particle region, agreement with Shires-Stevens in the small-particle region, and disagreement with Jones et al., Hardee and Nilson, and Dhir and Catton in the small-particle region. Gabor et al. (1981) used the Ergun equation and an experimental constant to evaluate the dryout heat flux for beds of small to large particles.

In research for the safety of nuclear reactors, various experimental works have been conducted for determining the dryout heat flux of porous beds. Ferrell and Alleavitch (1970) investigated the dryout heat flux of a pool boiling from a horizontal surface covered with a bed of unconsolidated particles confined by a screen to prevent movement of the particles. Dryout heat fluxes of different beds were obtained and methods were proposed for the prediction of heat transfer coefficients and dryout heat flux. Cornwell et al. (1976) used a thin polyurethane foam as the porous layer and boiled water by heating from the bottom. They used the fraction of vapor flow area to describe the heat flux. Jones et al. (1984) measured dryout heat fluxes of particulate beds heated from the base. Barleon and Werle (1981) measured dryout heat fluxes for both volumetric and bottom heatings.

The purpose of this paper is to analyze the pool boiling heat transfer from a flat horizontal heater that has a layer of fixed porous bed sintered on its surface. A dimensionless equation for the two-phase flow in a porous matrix was derived and solved. Experiments were also conducted to obtain boiling curves and heat transfer coefficients for methanol boiling under 1 atm pressure.

Experimental Method

An overall view of the experimental setup is shown in Figure 1a. A Pyrex glass cylinder of 60 mm ID and 180 mm length was used for the pool. The vapor produced was condensed and returned to the pool by the loop shown in the figure. The whole pool was nested inside another Pyrex glass pipe. The air temperature between the glass cylinders was controlled to near but less than the saturation temperature of the liquid to be boiled. At the bottom of the pool, a copper block of 40 mm dia. and 40 mm height, shown in Figure 1b, was inserted. The circular cross section that faced upward was sintered with spherical bronze particles of 115 to 150 mesh to form a layer of porous matrix. Sintering was carried out in a hydrogen furnace. Good contact between the base and the porous matrix was obtained. Porous matrices of different thickness were prepared. The copper block described above was heated by another larger copper block that had electrical heaters buried in it.

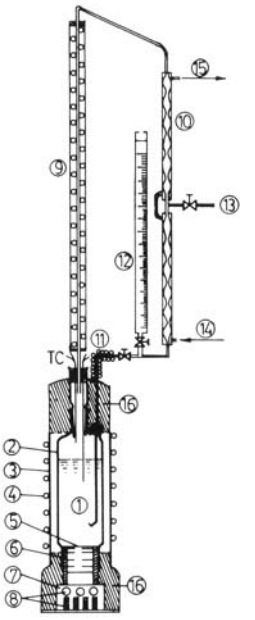

Figure 1a. Experimental setup.

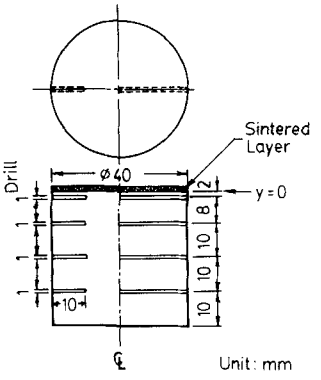

Figure 1b. Positions of thermocouples.

The temperatures of the copper block were monitored by copper-constantan thermocouples, as shown in Figure 1b. Heat flux was calculated by the temperature profile in the block. Temperatures were collected and stored by a data acquisition system comprising an AD/DA converter, a microcomputer, and its peripheral units.

Analysis

The following assumptions were made to analyze boiling from a heater that has a layer of porous bed:

• The porous layer may be treated as a fixed bed of granular solids

• Drying of the porous layer progresses upward from the heater surface when heating is from the base

• The equations for permeability and relative permeabilities adopted in the analysis are applicable to both the laminar and turbulent regions

• The friction factor adopted in the analysis is applicable when there are two phases present in the porous bed

• The porosity limitation on permeability and capillary pressure equations may be extended from 0.5 to 0.6 for cases where porosity is 0.6

• The properties of fluids are those at the boiling point and remain constant

• The granules in the porous layer have a representative particle diameter d_p

• The porous layer has porosity e, and an index of pore size distribution λ

The fluid properties used in this work are given in Table 1. Dryout heat flux is taken as the heat flux at which the relative liquid saturation at the heater surface is 0.

Lipinski (1981) and Gabor et al. (1981) applied a capillary pressure gradient equation to the problem of dryout heat flux in a porous medium. Different results were obtained for the dryout heat flux. In the following analysis, the derivation of the basic equations was included for the sake of completeness and convenience.

For a fluid flowing through a porous medium, the shear stress τ_w, pressure drop Δp, friction factor ϕ, the equivalent diameter d'_m, and the true velocity u_1, are related in a way analogous to that in the case of flow in a tube of diameter D. For the latter, this equation is

$$\tau_w = \frac{-\Delta p}{L}\frac{D}{4} = \phi \rho u_1^2 \tag{1}$$

For a porous medium, $D/4$ in the above equation is replaced by the equivalent diameter of the pore channel, d'_m. This diameter is related to bed porosity e and specific surface area s by (Coulson and Richardson, 1978)

$$d'_m = \frac{e}{s(1-e)}$$

Different equations are available for the friction factor; the factors are shown in Figure 2. The Ergun equation was developed from experimental data based on granular beds; it expresses the friction factor from laminar to turbulent flows in one equation. To make the results of this work applicable to the cases of granular beds, the Ergun equation, shown below, was used in this work

$$\phi = \frac{4.17}{Re_1} + 0.29 \tag{2}$$

where the Reynolds number is

$$Re_1 = \frac{\left[\dfrac{e}{s(1-e)}\right] u_1}{\nu}$$

Equation 2 is valid for $1 < Re_1/(1-e) < 2{,}000$. Substituting Eq. 2 into Eq. 1 using superficial velocity $u = u_1 e$, the following equations result

$$\frac{-\Delta p}{L} = \frac{\mu u}{\left[\dfrac{36e^3}{150s^2(1-e)^2}\right]} + \frac{1.75}{6}\frac{s(1-e)}{e^3}\rho u^2$$

$$= \frac{\mu}{k}u + \frac{\beta}{k}\rho u^2 \tag{3}$$

where β and permeability k are as follows

$$\beta = 1.75 d_p/[150(1-e)] \tag{4a}$$

$$k = d_p^2 e^3/[150(1-e)^2] \tag{4b}$$

The first term on the righthand side of Eq. 3 is the laminar contribution corresponding to Darcy's equation; the second term is the turbulent contribution. For a porous bed with both vapor and liquid phases present, Eq. 3 is applied to each phase as follows

$$-\frac{dp_v}{dy} = \frac{\mu_v}{k_v}u_v + \frac{\beta}{k_v}\rho_v u_v |u_v| + \rho_v g$$

$$-\frac{dp_w}{dy} = \frac{\mu_w}{k_w}u_w + \frac{\beta}{k_w}\rho_w u_w |u_w| + \rho_w g$$

where the gravitational effect is also included. $|u_v|$ and $|u_w|$ are introduced to take into account the effect of direction on flows. Subtracting the second equation from the first and writing p_c for

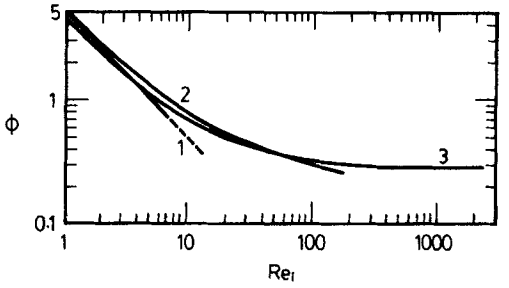

Figure 2. Friction factors.

1. Spherical particles; $\phi = 5/Re_1$ for $Re_1 < 2$
2. Spherical particles, Carman eq., $\phi = 5/Re_1 + 0.4/Re_1^{0.1}$ for $2 < Re_1 < 100$
3. Ergun eq., $\phi = 4.17/Re_1 + 0.29$ for $1 < Re_1/(1-e) < 2{,}000$

Table 1. Physical Properties of Fluids

Property	Methanol	Water	R-113*
ρ_w kg/m^3	751	958.3	1,511.0
ρ_v kg/m^3	1.222	0.5977	7.385
c_p	614.57	1,603	204.6
ν_w m^2/s	4.341 E-7	2.95 E-7	3.38 E-7
ν_v m^2/s	9.084 E-6	2.02 E-5	1.45 E-6
c_v	4.779 E-2	1.46 E-2	0.233
h_{fg} kJ/kg	1,101	2,257	146.8
σ N/m	1.875 E-2	5.878 E-2	1.48 E-2

*Freon 113

$(p_v - p_w)$, the capillary pressure gradient is then expressed by

$$-\frac{dp_c}{dy} = \left(\frac{\mu_v u_v}{k_v} - \frac{\mu_w u_w}{k_w}\right) + \beta\left(\frac{\rho_v u_v |u_v|}{k_v} - \frac{\rho_w u_w |u_w|}{k_w}\right) - \Delta\rho g \quad (5)$$

When the liquid permeating the porous matrix is balanced by the liquid evaporated, the mass balance equation is

$$\rho_w u_w + \rho_v u_v = 0 \quad (6)$$

Heat flux q is

$$q = \rho_v u_v h_{fg} \quad (7)$$

Substituting Eqs. 6 and 7 into Eq. 5 and rearranging the resulting equation, the following dimensionless equation is obtained

$$-\frac{dp_{cd}}{dy_d} = B\left(\frac{c_v}{k_{rw}} + \frac{1}{k_{rv}}\right) + B^2\psi\left(\frac{1}{c_\rho k_{rw}} + \frac{1}{k_{rv}}\right) - 1 \quad (8)$$

where

$$p_{cd} = p_c/\Delta\rho\, gL \quad (9a)$$

$$B = qv_v/(h_{fg}k\Delta\rho\, g) \quad (9b)$$

$$\psi = \beta k\Delta\rho g/(\rho_v \nu_v^2) = \frac{1.75}{150^2}\left(\frac{d_p e}{1-e}\right)^3\left(\frac{\Delta\rho\, g}{\rho_v \nu_v^2}\right) \quad (9c)$$

$$c_\nu = \nu_w/\nu_v \quad (9d)$$

$$c_\rho = \rho_w/\rho_v \quad (9e)$$

$$y_d = y/L \quad (9f)$$

$$k_{rw} = k_w/k \quad (9g)$$

$$k_{rv} = k_v/k \quad (9h)$$

B is the dimensionless heat flux. The parameter ψ relates d_p and e of the porous layer to the fluid properties. c_ν and c_ρ are the ratios of kinematic viscosity and density. The dimensionless distance y_d is 0 at the base of the bed. k_{rw} and k_{rv} are the relative permeabilities of the liquid and vapor and are expressed by (Corey, 1977)

$$k_{rw} = Se^n \quad (10a)$$

$$k_{rv} = (1 - Se)^2(1 - Se^m) \quad (10b)$$

where

$$n = 3 + 2/\lambda \quad (11a)$$

$$m = 1 + 2/\lambda \quad (11b)$$

λ is an index of pore size distribution and is determined by experiment. The relative liquid saturation Se is related to the absolute saturation S, maximum saturation S_m, and residual saturation S_r by the following equation

$$Se = \frac{S - S_r}{S_m - S_r} \quad (12)$$

Different equations are available for relating the capillary pressure and the saturation. Here, Udell's (1985) correlation equation of Leverett's experimental data, as shown below, was used.

$$L_d p_{cd} = \frac{p_c}{\sigma}\sqrt{\frac{k}{e}} = f(Se) \quad (13)$$

where

$$f(Se) = a(1 - Se) - b(1 - Se)^2 + c(1 - Se)^3 \quad (14a)$$

$$L_d = \frac{\Delta\rho\, gL}{\sigma}\sqrt{\frac{k}{e}} \quad (14b)$$

a, b, and c are given in the Notation; L_d is the dimensionless thickness of the porous layer.

Equation 13 is substituted into Eq. 8 and the resulting equation, after separating the variables, is integrated as follows

$$\int_{Se_o}^{Se} \frac{a - 2b(1 - Se) + 3c(1 - Se)^2}{B\left(\frac{c_v}{k_{rw}} + \frac{1}{k_{rv}}\right) + B^2\psi\left(\frac{1}{c_\rho k_{rw}} + \frac{1}{k_{rv}}\right) - 1} dSe = \int_0^{y_d} L_d dy_d = L_d y_d \quad (15)$$

The lower limit Se_o at $y_d = 0$ is a value between 1 and 0. $Se_o = 0$ indicates dryout. The Se value at the upper limit $y_d = 1$ is Se_L and this value has to be determined. Once Se_L is determined, Eq. 15 may be integrated for a given ψ at various B and Se_o.

The following method was used to find Se_L. The capillary pressure at any point is expressed by the following equation

$$p_c = \frac{4\sigma}{d} \quad (16)$$

where d is twice the radius of curvature of a meniscus at that point. At $y = 0$, d is d_o, and at $y = L$, d is d_L. Substitute Eq. 16 for p_c and Eq. 4b for k into Eq. 13 and write the resulting equation in the following form

$$\frac{d}{d_p} = \frac{4}{\sqrt{150}\, f(Se)}\frac{e}{1-e} \quad (17)$$

This equation is plotted in Figure 3a with Se as the parameter. For a given d_p, decreasing d/d_p means decreasing radius of curvature of a meniscus and increasing capillary pressure. When $y = 0$, and $Se = Se_o = 0$, and for example, for $e = 0.5$, then $d/d_p = d_o/d_p = 0.583$ is read from Figure 3a, and therefore $d_o = 0.583d_p$. Thus, if $d_L > 0.583d_p$, then by Eq. 16, $p_{c,L} < p_{c,o}$, the capillary pressure gradient is negative, and therefore the liquid flow is downward. However, if $d_L < 0.583d_p$, then $p_{c,L} > p_{c,o}$, the capillary pressure gradient is positive, and therefore liquid flow

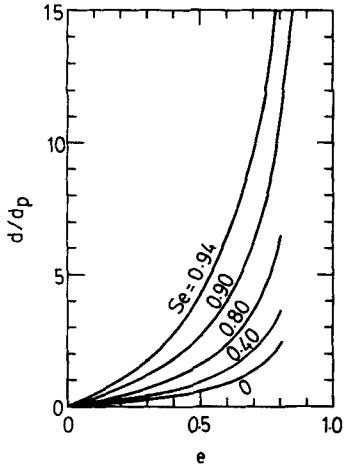

Figure 3a. Plot of Eq. 17.

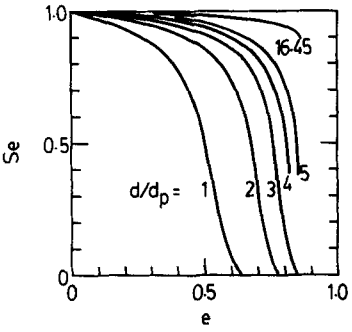

Figure 3b. Effect of d/d_p ratio on Se_L at various porosities.

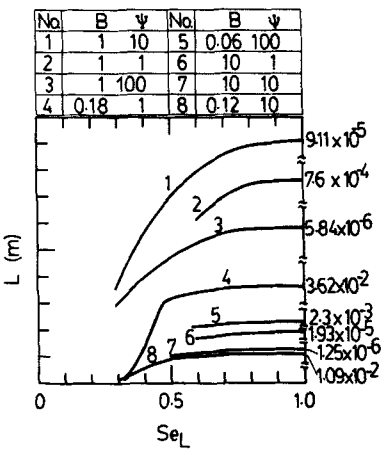

Figure 3c. Effect of Se_L on integration of Eq. 15.

downward is prevented. Before the dryout, liquid is transported to the heater surface from the top, therefore the liquid flow is downward and the capillary pressure gradient is negative. Thus, for porosities between 0.3 and 0.6, d_L should be more than several times d_p. For example, with $e = 0.5$, if we assume $d_L/d_p = 4.205$, then, by Figure 3a it is found that $Se_L = 0.94$. The effect of the d_L/d_p ratio on Se_L vs. e is shown in Figure 3b. For small d_L/d_p, for example, for $d_L/d_p = 1$, Se_L depends strongly on porosity and can be negative when porosity exceeds 0.63. As d_L/d_p increases, the effect of porosity on Se_L diminishes. For $d_L/d_p = 16.45$, which is obtained for beds of small particles, say, $d_p = 0.1$ mm, by assuming $d_L = d_b$, where d_b is the diameter of a departing bubble of, say, 1.645 mm, then Se_L is almost independent of porosity and has a value between 0.96 and 0.99 for porosities between 0.3 and 0.6. For beds of large particles, resistance to liquid permeation is small and d_L is considered to be at least several times greater than d_p. The effect of the magnitude of Se_L on the integration of Eq. 15 is shown in Figure 3c. For $Se_L > 0.8$, the effect is negligible. Therefore, in this work, unless otherwise noted, $Se_L = 0.95$ was used. Now Eq. 15 can be integrated for a given ψ to give a relation between L_d and B for various Se_o.

The Reynolds number, which does not appear explicitly in Eq. 15, is related to the dimensionless groups B and ψ as follows. For the vapor phase, the Reynolds number is

$$Re_{1,v} = \frac{\left[\frac{e}{s(1-e)}\right] u_{1,v}\rho_v}{\mu_v} \tag{18}$$

Substitution of $s = 6/d_p$ and $u_{1,v} = u_v/e$ into the above equation results in

$$Re_{1,v} = \frac{B}{6 \times 150}\left[\frac{d_p e}{(1-e)}\right]^3 \left(\frac{\Delta\rho\, g}{\rho_v \nu_v^2}\right)$$

Substituting Eq. 9c into the above equation results in

$$Re_{1,v} = \left(\frac{150}{6 \times 1.75}\right) B\psi \tag{19}$$

This equation relates the dimensionless quantities $Re_{1,v}$, B, and ψ, and is independent of fluid. For small particles, ψ is small, $Re_{1,v}$ tends to be small even for large B, and the vapor flow is likely to be laminar. For large particles, ψ is large, $Re_{1,v}$ tends to be large even for moderate B, and the vapor flow is likely to be in the transition and turbulent regions.

Similarly, for the liquid phase, the Reynolds number is

$$Re_{1,w} = \frac{\left[\frac{e}{s(1-e)}\right] u_{1,w}\rho_w}{\mu_w} \tag{20}$$

therefore

$$Re_{1,w} = \frac{B}{6 \times 150}\left(\frac{d_p e}{1-e}\right)^3 \left(\frac{\Delta\rho\, g}{\rho_v \nu_v^2}\right)\left(\frac{\rho_v \nu_v}{\rho_w \nu_w}\right) \tag{21}$$

Substitution of Eq. 9c into the above equation results in

$$Re_{1,w} = \left(\frac{150}{6 \times 1.75}\right) B\psi \left(\frac{\rho_v}{\rho_w}\frac{\nu_v}{\nu_w}\right) \tag{22}$$

Comparison of Eqs. 19 and 22 shows that Reynolds numbers for the vapor and liquid phases are related by

$$Re_{1,w} = \frac{Re_{1,v}}{\left(\frac{\rho_w}{\rho_v}\frac{\nu_w}{\nu_v}\right)} \tag{23}$$

For water and methanol boiling under 1 atm pressure, $\rho_w\nu_w/\rho_v\nu_v$ are 23.41 and 29.37, respectively.

The thickness of the porous bed is reflected by the denominator of the integrand on the lefthand side of Eq. 15. When this denominator is zero

$$B\left(\frac{c_v}{k_{rw}}+\frac{1}{k_{ro}}\right)+B^2\psi\left(\frac{1}{c_p k_{rw}}+\frac{1}{k_{ro}}\right)-1=0 \qquad (24)$$

L is infinite. This equation relates B to Se for very thick porous layers of different characteristics. It is a quadratic equation for B and may be solved for various given values of ψ. The maximum B, B_{max}, obtained from Eq. 24 is, as will be shown later in the discussion, the dimensionless dryout heat flux, B_{dry}, for a very thick porous layer.

Two limiting cases exist for Eq. 15. The first limiting case is that only the laminar contribution is important. This corresponds to the case $\psi = 0$. Although, by definition ψ cannot be zero, this limiting case is approached as $\psi \to 0$. Both liquid and vapor flows are laminar in this case. Beds with small particle diameters tend toward this condition. Equation 24 can then be written as

$$B=\frac{1}{\left(\frac{c_v}{k_{rw}}+\frac{1}{k_{ro}}\right)} \qquad (25)$$

which shows that B is dependent on c_p, λ, and Se. B_{max} of the above equation is the B_{dry} of a very thick bed with laminar flows.

The second limiting case is in the high-turbulence region where the laminar contribution is negligible. The friction factor, as shown in Eq. 2, is a constant. Beds with large particle diameters tend toward this condition. Equation 24 is then rewritten as

$$(B\sqrt{\psi})_T=\left(\frac{1}{\frac{1}{c_p k_{rw}}+\frac{1}{k_{ro}}}\right)^{0.5} \qquad (26)$$

where the subscript T indicates this limiting case. $(B\sqrt{\psi})_T$ depends on c_p, λ, and Se. The B_{max} of the above equation is again the B_{dry} of a very thick bed with very high turbulent flows.

The effect of particle diameter on the dryout heat flux can be analyzed as follows. Recalling the definition of B, B_{max} is then written as

$$B_{max}=\frac{q_{dry}\,\nu_v}{h_{fg}k\Delta\rho\, g} \qquad (27)$$

Rewrite the above equation for q_{dry}; then

$$q_{dry}=B_{max}\frac{1-e}{d_p}\left(\frac{150}{1.75}\rho_v\nu_v h_{fg}\psi\right) \qquad (28)$$

This equation may be written in two forms for the two limiting cases. The first form is

$$\log q_{dry}=\log\left[\frac{B_{max}h_{fg}\Delta\rho\, g\, e^3}{150\nu_v(1-e)^2}\right]+2\log d_p \qquad (29)$$

As $L \to \infty$ and $\psi \to 0$, B_{max} approaches a constant. Therefore, the above equation shows that for a very thick bed of given characteristics and given fluid properties, $\log q_{dry}$ vs. $\log d_p$ for a given porosity approaches a straight line of slope 2 as $\psi \to 0$. The second form is

$$\log q_{dry}=\log\left[h_{fg}\sqrt{\frac{\rho_v\Delta\rho g e^3}{1.75(1-e)}}\,B_{max}\sqrt{\psi}\right]+\frac{1}{2}\log d_p \qquad (30)$$

As $L \to \infty$ and $\psi \to \infty$, then $B_{max}\sqrt{\psi} \to (B\sqrt{\psi})_T$. Therefore, Eq. 30 shows that for a very thick bed of given characteristics and a given fluid, $\log q_{dry}$ vs. $\log d_p$ for a given porosity approaches a straight line of slope $1/2$ as $\psi \to \infty$. Between the two limits, Eqs. 28 and 9c can be used to plot $\log q_{dry}$ vs. $\log d_p$ for a given porosity at various ψ.

Results and Discussion

The results are discussed in three sections: experiment, $\psi = 0$ case, and $\psi > 0$ case.

Experiment

The experimental boiling curves of methanol in a pool heated by a copper block with its horizontal flat surface sintered with a thin layer of porous matrix are shown in Figure 4a. For comparison, the boiling curve of a smooth surface is also shown in the figure. The degree of enhancement in heat transfer depends on the thickness of a porous layer, symbolized by L/d_p. When L/d_p is about 2, the enhancement is most pronounced. The critical heat flux (CHF) is 900 kw/m^2, compared to 600 kw/m^2 for the smooth surface. At a still greater L/d_p, heat transfer is enhanced in the region where q is relatively low but diminished in the region where q is relatively high, although the CHF is still about 900 kw/m^2. When L/d_p is about 10 or more, corresponding to about 1 mm or more in thickness, boiling curves show a clear reduction in slope, indicating a rapid increase in heater surface temperature relative to the heat flux. This is due to an insufficient supply of liquid through the matrix and the onset of dryout in the porous layer.

The heat transfer coefficient h is calculated from the experi-

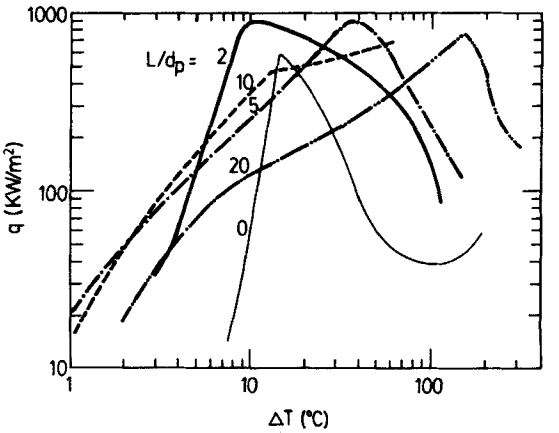

Figure 4a. Boiling curves of methanol.

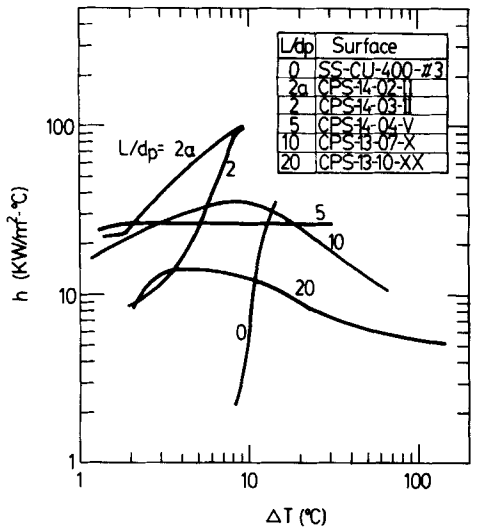

Figure 4b. Heat transfer coefficient, methanol.

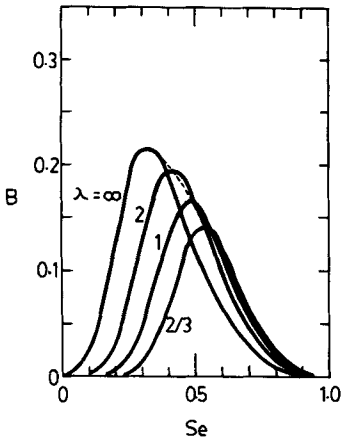

Figure 5a. Heat flux vs. relative liquid saturation, methanol.
Thick porous matrices of different pore size distribution index.

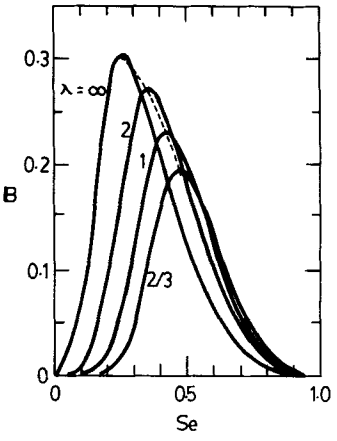

Figure 5b. Heat flux vs. relative liquid saturation, water.
Thick porous matrices of different pore size distribution index.

mental data and is shown in Figure 4b. For porous layers with thickness about $2d_p$, as shown by curve 2 in the figure, h is very high and varies considerably with the degree of superheat. CHF occurs at superheat of about 9 K. For thickness about $5d_p$, h is shown to be relatively constant and the superheat at CHF is about 30 K. When the thickness is about $10d_p$, h increases to the dryout point and then decreases. The superheat at CHF is about 65 K. For a thick layer of about $20d_p$, h reduces further and the superheat of CHF is about 140 K.

In Figure 4b the difference between curves 2 and 2a shows that a sintering method that will warrant a specific porous structure is important. The boiling curves and h are affected by the arrangement of particles in the porous layer. The particle arrangement may alter during the sintering process. Rearrangement of particles during sintering may cause the sintered porous matrices to be of different characteristics even though the particles used for sintering come from the same batch. This effect is most pronounced when the layer is thin. Another factor that influences the characteristics of the porous layer is the size distribution of the particles used. In many investigations, particles of a certain size range were used. Permeability of the matrix is greatly affected by the size distribution of the particles. In theoretical work, permeability is often computed by using a representative particle diameter and porosity.

$\psi = 0$ *case*

This is the case where the fluid flows are laminar and the turbulent term as shown by the second term in Eq. 3 is neglected.

For very thick porous beds, Eq. 25 is applicable. Figures 5a and 5b show the plot of this equation for methanol and water. The dimensionless heat flux B depends on the relative saturation Se and the pore size distribution parameter λ. It has been shown by Brooks and Corey (1966) that for a typical porous medium, $\lambda = 2$; for soils with well developed structures, $\lambda < 2$; for uniform pore size structure, $\lambda \rightarrow \infty$; and for porous media that have secondary porosity, that is, pore spaces available for flow within the aggregates in addition to primary porosity, λ as low as 0.46 was obtained. These figures show that a small λ has a more pronounced effect on the curves than a large λ. The broken-line curves in Figures 5a and 5b are the loci of maximum B. B_{max} increases as λ increases, while the corresponding liquid saturation, Se_{max}, decreases. In the following text, unless otherwise noted, $\lambda = 2$ is used.

In Eq. 15, the thickness of the bed is related to the dimensionless heat flux. For methanol, this relation is shown in Figure 6 as L vs. B for a given Se_L and various Se_o. The solid curves are for the case of porosity 0.5. For a porous bed of given thickness, as the heat flux increases, Se_o decreases and finally becomes zero. The B value read on the curve with $Se_o = 0$ is the dimensionless dryout heat flux, B_{dry}, for that thickness. When the bed thickness increases, B_{dry} decreases. This phenomenon was observed in the experiments. Figure 4a shows that when L/d_p increased from 10 to 20, the dryout heat flux decreased from 470 to 120 kw/m^2. In Figure 6, with the increase in L, curves with $Se_o \leq Se_{max}$ converge to the B_{dry} curve. When L is sufficiently large, B_{dry} eventually approaches B_{max} and becomes independent of L, as indicated by the steep increase in L in the figure. Thus, for thick beds of the same characteristics, B_{dry} is independent of thickness and is equal to B_{max}. Figures 5a and 5b show that the maximum of B_{max}, and therefore of B_{dry}, occurs when $\lambda = \infty$. In Figure 6, for curves with $Se_o > Se_{max}$, as the bed thickness increases the

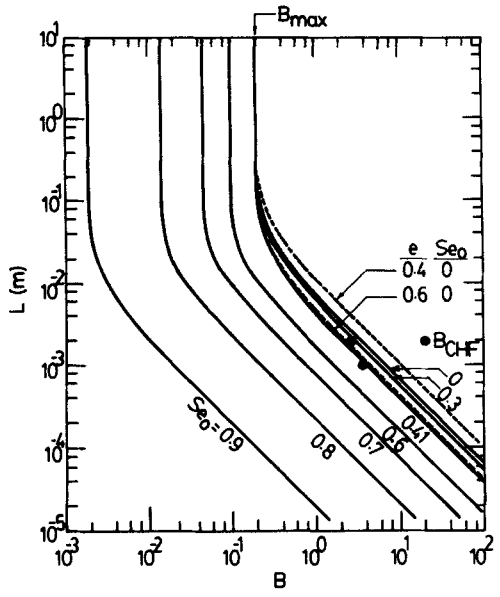

Figure 6. Porous layer thickness vs. heat flux at various liquid saturations at heater surface, methanol.
$e = 0.5$; $d_p = 100\ \mu m$; $Se_L = 0.9857$; $\lambda = 2$
---- Dryout heat flux at indicated porosities

dimensionless heat flux decreases toward a particular value. This particular B is the ultimate dimensionless heat flux for that thick porous matrix at that specific value of Se_o and is depicted by the curve with $\lambda = 2$ in Figure 5a by taking $Se = Se_o$ on the abscissa. Thus, Figure 6 indicates that for a porous matrix of thickness about several cm or more, the dimensionless heat fluxes before and at dryout are independent of thickness.

For thick porous beds of small particles, theoretical and empirical equations for the dryout heat flux have been proposed by investigators in the researches for the safety of nuclear reactors. In Table 2 these equations are shown in dimensionless forms. The values of B_{dry} for water and methanol were calculated by these equations. B_{dry} by Bau and Torrance's equation is greater than others. This may be due to the negligence of capillary pressure. Udell's results correspond to the case of $\lambda = \infty$. The equation proposed by Jones et al. is a correlation equation of their experimental data. Their equation corresponds to the case of $\lambda = 0.6$. The dimensionless dryout heat fluxes of porous beds by volumetric heating, B_v, are also shown in the table. The equation of Hardee and Nilson and that of Bau and Torrance are essentially the same except for the density factor, $\rho_w/\Delta\rho$, which has a value close to 1. The values of B_v shown in the table are all greater than the B_{dry} of this investigation. As the value of λ is not given in most investigations, it can only be pointed out that the ratio of B_v/B_{dry} is, from the table, around 2 and 3. The equations of Gabor et al. (1981) for bottom and volumetric heatings indicate that this ratio is 2. It has been generally accepted that for thick beds of small particles, log q_{dry} vs. log d_p is a straight line of slope 2, as is indicated by Eq. 29. However, this equation also shows that the intercept is dependent on the fluid properties, porosity, particle diameter, and pore size distribution parameter. A plot of Eq. 29 for water boiling with thick porous beds of different pore size distribution index λ is shown in Figure 7. The effect of λ on the dryout heat flux is great when λ is small, but this effect decreases as λ increases. The dryout heat flux

Table 2. Equations for Predicting Dimensionless Dryout Heat Flux for Thick Porous Matrix
$\psi = 0$ or beds of small particles where fluid flows are laminar.

No.	Eq.	B_{dry} Methanol	B_{dry} Water	Ref.
1	$B_{dry} = \frac{5}{6}\frac{1}{(1+\sqrt{c_v})^2}$	0.5612	0.6623	Bau & Torrance (1982)
2	$B_{dry} = \frac{1}{(1+c_v^{0.25})^4}$	0.2156	0.3032	Udell (1985)
3	$B_{dry} = \frac{5}{6}\frac{0.015/c_v^{0.8}}{(1+0.003/c_v^2)^{0.25}}$	0.1154	0.1866	Jones et al. (1984)
4	$B_{dry} = \left(\frac{1}{c_v/k_{rw}+1/k_{ro}}\right)_{max}$	λ: 0.2155 (∞); 0.1943 (2); 0.1657 (1); 0.1414 (2/3); 0.1145 (0.45)	λ: 0.3032 (∞); 0.2724 (2); 0.2311 (1); 0.1964 (2/3); 0.1864 (0.6)	This work
5	$B_v = \frac{5}{6}\frac{1}{(1+\sqrt{c_v})^2}\frac{\rho_w}{\Delta\rho}$	0.5615	0.6627	Hardee & Nilson (1977)
6	$B_v = 0.01473\frac{1}{c_v}\sqrt{\frac{\rho_w}{\Delta\rho}}$	0.3085	1.0091	Dhir & Catton (1982)
7	$B_v = \frac{5}{6}\frac{1}{[1/(1-1.11\gamma)+c_v/\gamma^3]}$, $\gamma = [0.833\,c_v + \sqrt{2.7\,c_v}]^{0.5} - (0.833\,c_v)^{0.5}$	0.3315	0.4217	Lipinski (1980)

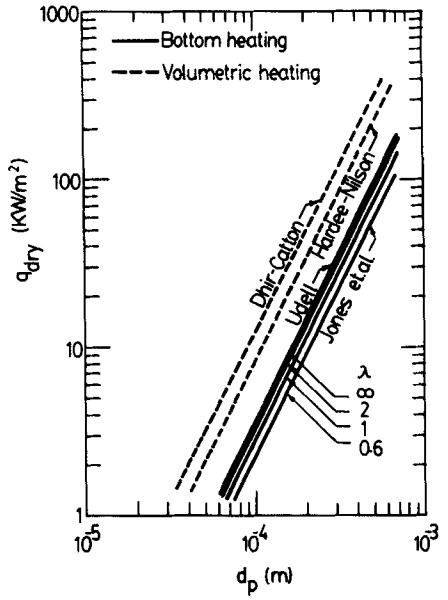

Figure 7. Effect of pore size distribution index on dryout heat flux vs. particle diameter, water.
Thick porous matrix; porosity 0.4, $\psi \to 0$

increases 1.6-fold when λ changes from 0.6 to ∞. The cases of Udell and Jones et al. are shown in Figure 7; for comparison, the cases of volumetric heating are also shown.

In contrast to the thick porous layer, Figure 6 shows that B increases with decreasing L. Liquid supply to the heater surface is easier when the porous layer is thin. In the figure, the dimensionless critical heat flux, B_{CHF}, obtained from this experiment is indicated for the case of $L = 2$ mm. The relative position of B_{CHF} to B_{dry} is an indication of how soon the dryout occurs in a porous layer during boiling.

In Figure 6, the broken-line curves are the dimensionless dryout heat flux for the cases of porosities 0.4 and 0.6. For a porous bed packed with uniform spherical particles, the porosity ranges from 0.4764 to 0.2595 for cubic to rhombohedral packings. However, in a sintered bed, a porous bed with structure may be developed and the pore space is then the sum of the primary pore space and the secondary pore space. Porosity may exceed 0.5. Afgan et al. (1985) showed that for their porous layers, porosity ranged from 0.3 to 0.7. In Figure 6, for a given L, a bed with large porosity has smaller B_{dry}. The results of our experimental work for methanol are also shown. Porosities of 0.54 and 0.65 were used respectively for 1 and 2 mm thick porous layers.

Figure 8 shows the dimensionless bed thickness L_d vs. B_{dry} for methanol and water. For the same L_d, water has larger B_{dry} than methanol. The experimental data for water by Ferrell and Alleavitch (1970) are shown in the figure for comparison. Their data were obtained from beds of confined and unconsolidated Monel metal particles of respective average diameters of 505 and 357 μm. The value of L/d_p for each datum point is indicated. These data points show that B_{dry} decreases with increasing L/d_p, as was expected. However, it is also shown that data points of larger particles are closer to the laminar curve. For large particles, the pores are also large and the flow can be different from the small-particle case. For the latter, laminar flow prevails. This apparently inconsistent result may be due to the particles, which are not one size but have a size distribution. The results of our experimental work for methanol are also shown.

Afgan et al. (1985) investigated the boiling of water from

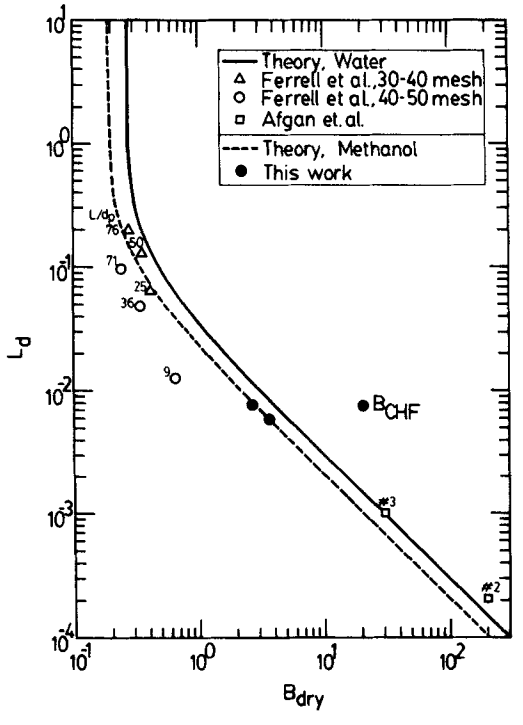

Figure 8. Thickness of porous layer vs. dryout heat flux, methanol and water.
λ = 2

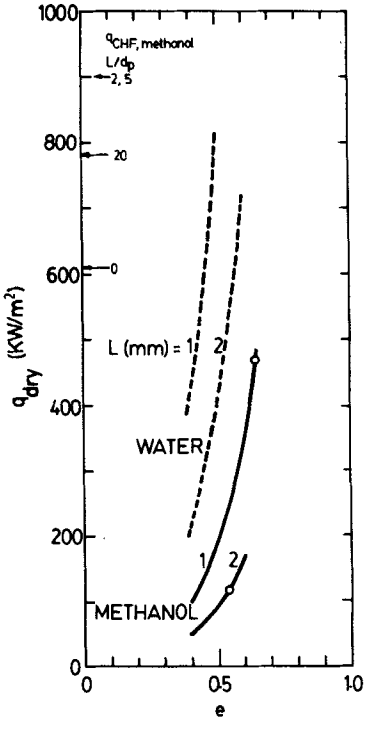

Figure 9. Effects of porous layer thickness and porosity on dryout heat flux.
λ = 2; d_p = 100 μm

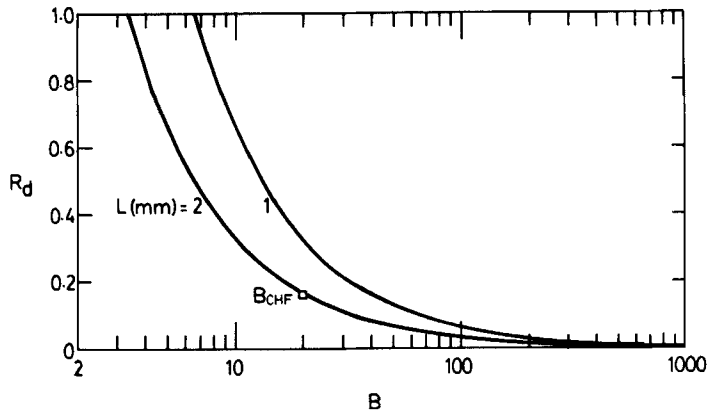

Figure 10. Thickness of wet zone vs. heat flux, methanol.
Porosity 0.5; $\lambda = 2$

horizontal tubes sintered with spherical metal particles of 63 to 100 μm size. Their boiling curves for large tubes of 16 and 18 mm dia., sintered respectively with porous layers of 2.2 and 0.55 mm thickness, show apparent change in slope at more than one point. These points, not shown here, fall far to the left of the water curve in Figure 8. For small tubes of 3 and 4 mm dia., sintered with 0.45 and 1.5 mm thick porous layers, data points #2 and #3 were obtained by taking q_{dry} equals to 500 and 230 kw/m^2, respectively, from the boiling curves. The effect of tube diameter on boiling is important but not well understood.

The effect of porosity on dryout heat flux is shown in Figure 9. For a given bed thickness, the bed with a larger porosity, that is, with a higher permeability, is less easy to dry out, and therefore has a larger dryout heat flux. For a given porosity, a thin porous bed is less easy to dry out and therefore the dryout heat flux is higher. The dryout heat flux with water is greater than methanol. The critical heat fluxes of methanol from this experiment are indicated on the figure for reference.

Once dryout is initiated at the bottom of the porous layer, the thickness of the liquid layer decreases as the heat flux is increased. In Figure 10, for methanol, the dimensionless thickness of the wet zone, R_d, is plotted against B. R_d is the ratio of the wet zone thickness to bed thickness L. B_{CHF} for $L = 2$ mm is indicated in the figure and is seen to occur when $R_d = 0.16$, that is, at a depth of about three particle diameters. The real situation is likely to be more complex than can be indicated by this figure.

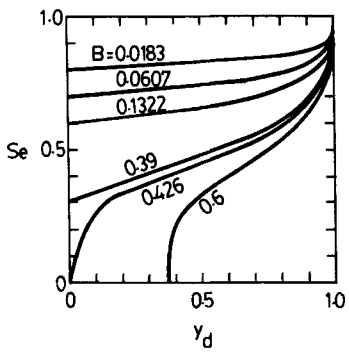

Figure 11. Distribution of liquid saturation in a porous matrix at various heat flux values, methanol.
$L = 5.1 \times 10^{-2}$ m; $\lambda = 2$

Figure 11 shows the distribution of liquid saturation Se in a porous bed at various dimensionless heat fluxes. Liquid saturation is relatively uniform when B is small. Dryout occurs at $B = 0.426$. Then the dry zone increases with increasing B.

$\psi > 0$ case

For $\psi > 0$, both laminar and turbulent contributions are accounted for. For small ψ, the situation is close to the previous case of $\psi = 0$. For very large ψ, only the turbulent contribution is important. Between these two extreme cases, the transition region exists. It has been shown that ψ, d_p, and e are related by Eq. 9c. The order of magnitude of ψ for a given particle diameter and porosity can be sized quickly by Figure 12 for methanol and water.

In Eq. 19, ψ is related to the Reynolds number and the dimensionless heat flux B. Figure 13 shows this relation. When $Re_{1,v}$ is less than 2, both the vapor and liquid flows are laminar. This is the case for small ψ with any B of practical situation, or for large ψ with small B. For $2 < Re_{1,v} < 100$, the vapor flow is in the transition region, while the liquid flow is in the laminar or tran-

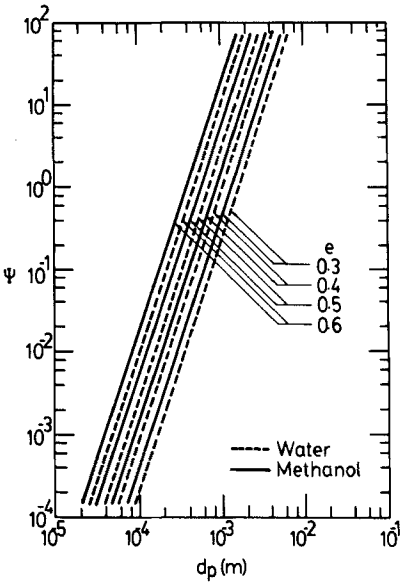

Figure 12. ψ vs. particle diameter at various porosities.

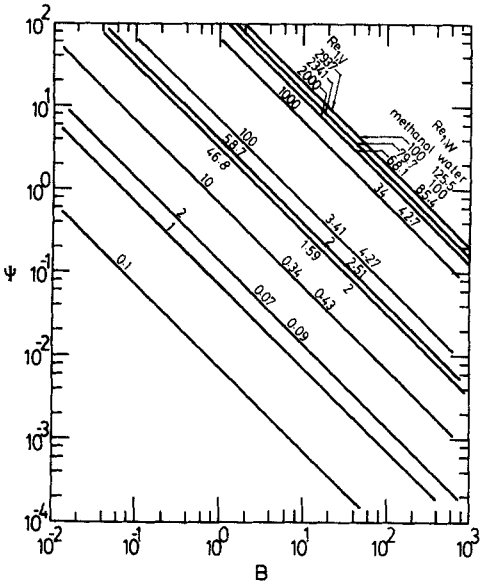

Figure 13. ψ related to heat flux and Reynolds numbers.

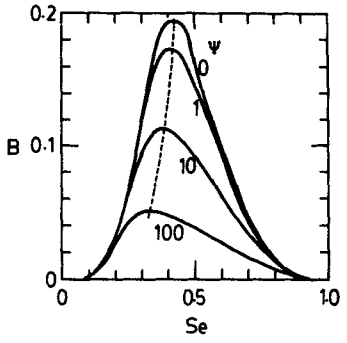

Figure 14a. Heat flux vs. relative liquid saturation at various ψ, methanol.
Thick porous matrix; $\lambda = 2$

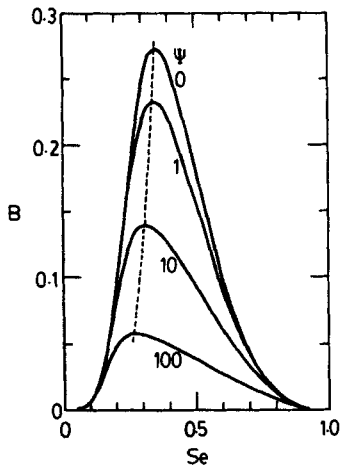

Figure 14b. Heat flux vs. relative liquid saturation at various ψ, water.
Thick porous matrix; $\lambda = 2$

sition region. For the same $Re_{l,v}$, $Re_{l,w}$ for water is greater than $Re_{l,w}$ for methanol. For thin porous layers, the experimental values of B are about or less than 100. Therefore, for $Re_{l,w}$ to be greater than 100, ψ must be greater than 1.6 for water and 2 for methanol. For thick porous layers, the experimental values of B_{dry} for water are less than 0.8. Therefore, for water, to have $Re_{l,w}$ greater than 100, ψ should be about 1,000 or more. In most experiments, the vapor phase is in laminar, transition, or turbulent regions, while the liquid phase is in laminar or transition regions.

Figures 14a and 14b show the solution of Eq. 24 for very thick porous layers with methanol and water, respectively. The curve with $\psi = 0$ represents the previous case. This curve is the upper limit of all other curves. As ψ increases, both B_{max} and Se_{max} decreases. The broken-line curve is the locus of B_{max}.

In Figures 15a and 15b the solution of Eq. 24 is compared with that of Eq. 26, that is, with the case of high turbulence with laminar contribution totally neglected. Curve T is the plot of Eq. 26 and is the upper limit of all other curves. This figure shows that even with $\psi = 10^4$, the limiting situation is not quite attained. The ratios of the ordinates of each curve to that of curve T were plotted in Figure 16 for water. The degree of turbulence contribution is shown to depend on Se. The effect of turbulence is more significant for Se around 0.5 than for low or high Se.

In Figure 17, the B values obtained from Eq. 24 are compared with those obtained from Eq. 26 for water. It is shown that even with $\psi = 1{,}000$, the two curves do not quite overlap, especially in the region of small Se. When $\psi = 100$, the laminar contribution is still quite important. Therefore, one should be cautious when only the turbulent term is used to describe the problem. The

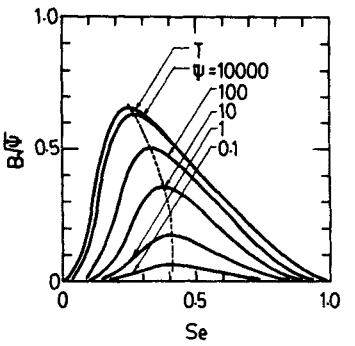

Figure 15a. $B\sqrt{\psi}$ vs. Se at various ψ, methanol.
Thick porous matrix; $\lambda = 2$

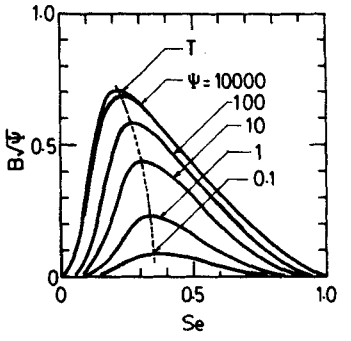

Figure 15b. $B\sqrt{\psi}$ vs. Se at various ψ, water.
Thick porous matrix; $\lambda = 2$

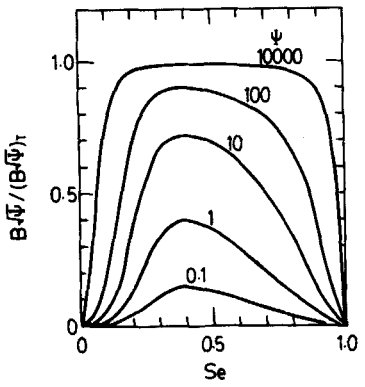

Figure 16. Effect of ψ on $B\sqrt{\psi}$ at various *Se*, water.
Thick porous matrix; $\lambda = 2$

result can be an overestimate of the real situations where the laminar contribution is still important.

The effect of pore size distribution index, λ, on the plot of $(B\sqrt{\psi})_T$ vs. *Se* is shown in Figure 18a for methanol and in Figure 18b for water. The broken-line curves are the loci of maximum $(B\sqrt{\psi})_T$.

In Figures 19a and 19b, B_{max} and $B_{max}\sqrt{\psi}$ are plotted against ψ for methanol and water boiling with very thick porous layers of $\lambda = 2$. For water, Figure 19b shows that as ψ decreases, B_{max} increases to approach 0.2724, which was the value obtained in the $\psi = 0$ case. On the other hand, as ψ increases, $B_{max}\sqrt{\psi}$ approaches 0.7083, as calcualted by Eq. 26.

Figures 20a and 20b show the plot of dimensionless bed thickness vs. dimensionless dryout heat flux at various ψ in accordance with Eq. 15 for methanol and water. The effect of ψ is more pronounced in the region of small L_d than in the region of large L_d. The curves for constant $Re_{1,v}$ were constructed as follows. For the ψ values indicated in Figure 20b, the values of B were read from Figure 13 for a chosen value of $Re_{1,v}$. These sets of (ψ, B) were marked in Figure 20b and the points were connected by a dot-dash curve. To extend this curve to the region of large L_d, Eq. 19 was plotted in Figure 19b for that $Re_{1,v}$. The point of intersection of Eq. 19 with the B_{max} curve decides the

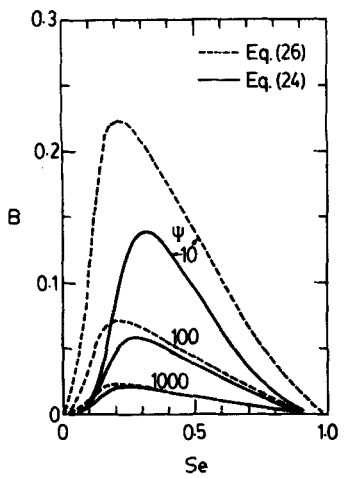

Figure 17. Comparison of heat flux calculated by Eqs. 24 and 26, water.
Thick porous matrix; $\lambda = 2$

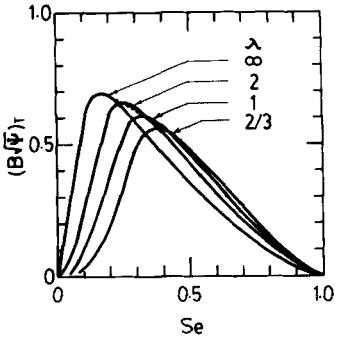

Figure 18a. Effect of pore size distribution index on $(B\sqrt{\psi})_T$ vs. *Se*, methanol.
Thick porous matrix; $\psi \to \infty$

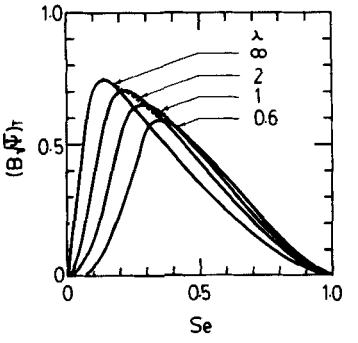

Figure 18b. Effect of pore size distribution index on $(B\sqrt{\psi})_T$ vs. *Se*, water.
Thick porous matrix; $\psi \to \infty$

(ψ, B) point when L_d is very large. This point together with the dot-dash curve forms a complete constant $Re_{1,v}$ curve. Constant Reynolds number curves of $Re_{1,v} = 2$, 10, 100, and 1,000 are shown in the figure. The curve with $Re_{1,v} = 2$ is very close to the drying curve of the $\psi = 0$ case. However, for greater $Re_{1,v}$ the curves spread out wider as $Re_{1,v}$ increases. The values of L/d_p and ψ of each datum point were tabulated and are shown in the data table at the top of the figures. The experimental data of Ferrell and Alleavitch (1970) for water fall in the region where $Re_{1,v} < 100$, and also in the region where $\psi < 10$. Their ψ values, as indicated by the data table, are not in accord with this analysis. That is, data points with larger ψ are closer to the laminar curve, and the magnitude of ψ of a datum point is quite different from the ψ value of the constant ψ curve nearest to it. This may be due to the distribution in the sizes of the particles. Chang and Kim (1985) tabulated the volumetric heating data of various investigators. These data are shown by open symbols in the figures. The values of L/d_p with ψ show qualitative agreement with this analysis although the heating mode is different. In Figure 20a, for methanol, the data of Tsai and Catton (1983) and Catton and Jakobsson (1987) were compared.

The prediction equations for q_{dry} proposed by various investigators were written in dimensionless forms for $B_{dry}\sqrt{\psi}$ and are tabulated in Table 3. The values of $B_{dry}\sqrt{\psi}$ for methanol and water were calculated by these equations. The results of this work's analysis are shown as Nos. 2 and 3 in the table. Number 3 shows that in the extreme case of turbulent flow, $B_{dry}\sqrt{\psi} \leq 0.7457$ for water and $B_{dry}\sqrt{\psi} \leq 0.6935$ for methanol. All values of $B_{dry}\sqrt{\psi}$ in No. 3 are about twice as large as those predicted by

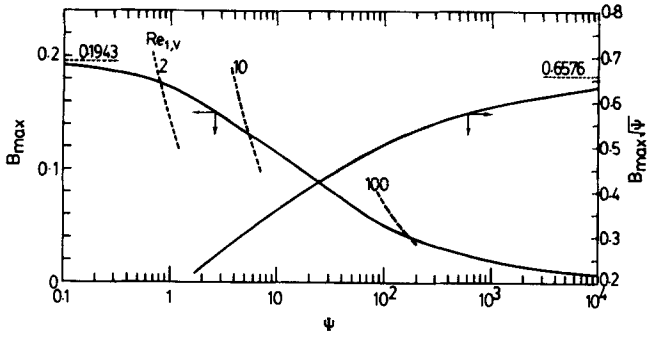

Figure 19a. Effects of ψ on B_{max} and $B_{max}\sqrt{\psi}$, methanol.
Thick porous matrix; $\lambda = 2$

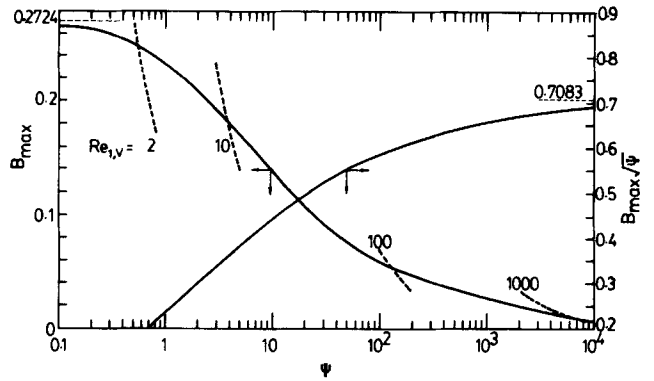

Figure 19b. Effects of ψ on B_{max} and $B_{max}\sqrt{\psi}$, water.
Thick porous matrix; $\lambda = 2$

No. 1, which when compared with No. 2 are shown to correspond to the $B_{max}\sqrt{\psi}$ at $\psi = 5.5$ for methanol, and to the $B_{max}\sqrt{\psi}$ at $\psi = 2.1$ for water. Number 4 is the result of Gabor et al. (1981) for bottom heating. Their limiting values are $(CB_{dry})_{\psi=0} = 1.2$ and $(CB_{dry}\sqrt{\psi})_{\psi=\infty} = 1.0$ for the liquids tested. C is an experimental constant, as shown in the table. Also shown in the table are the equations proposed for B_v, the dimensionless dryout heat flux for the case of volumetric heating. Comparison of No. 5 with No. 3 shows that Lipinski's (1980) result for volumetric heating corresponds to the case of bottom heating with $\lambda = \infty$ and considering only the turbulent term. This is not surprising in view of the similarity in equations. Lipinski (1981) also showed that the drying power predicted by the one-dimensional model is close to that predicted by No. 5 of the table. If $\lambda = \infty$ can be assumed for the bed, then the above comparison implies that at high turbulence the ratio B_v/B_{dry} is nearly 1. The values of $B_v\sqrt{\psi}$ predicted by Nos. 6 and 7 of Table 3 are about one-half to one-third of those predicted by No. 3.

In Figures 21a, 21b, and 21c, the dryout heat flux of a thick bed is plotted against the particle diameter in accordance with Eq. 28 for methanol, water, and Freon R-113. In the region of small ψ or small particle diameters, all curves become straight lines of slope 2, as shown by Eq. 29; and in the region of large ψ or large particle diameters, all curves approach straight lines of slope ½, as shown by Eq. 30. The departures from the linear behaviors of both limiting cases become clear at $\psi \simeq 0.1$ and $\psi \simeq$ 10,000.

Experimental data of dryout heat flux that can be found in the open literature are mostly in the region of $\psi > 0.1$ to $\psi < 10^5$, as shown in Figures 21a, 21b, and 21c. In the figures, (B) and

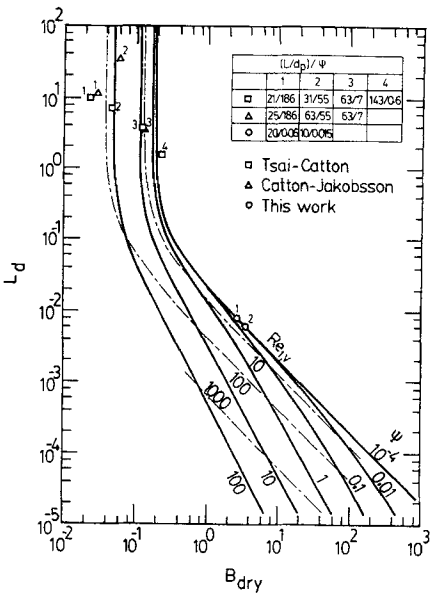

Figure 20a. Porous layer thickness vs. dryout heat flux at various ψ and vapor Reynolds number, methanol.
$\lambda = 2$

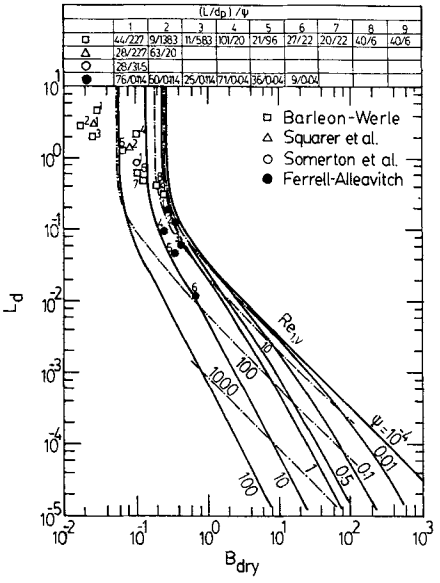

Figure 20b. Porous layer thickness vs. dryout heat flux at various ψ and vapor Reynolds number, water.
$\lambda = 2$

(V) indicate the bottom and volume heatings. Porosity is 0.4 or around that value. For water, as shown in Figure 21b, more data of volumetric heating are available than of bottom heating. For the latter, two data points for steel spheres with porosities 0.422 and 0.436 (Barleon and Werle, 1981) are shown. These points fall below the analytical curve of porosity 0.4. It is interesting to note that the volume heating data of several investigators (Chang and Kim, 1985) fall closely along the curve of porosity 0.4 in the transition region with $\psi > 10$. This trend is also observed for Freon-113. The experimental data of Catton and

Table 3. Equations for Predicting Dimensionless Dryout Heat Flux for Very Thick Matrices

$\psi \gg 0$ or beds of large particles where fluid flows are in transition to turbulent regions.

No.	Eq.	$B_{dry}\sqrt{\psi}$ Methanol	$B_{dry}\sqrt{\psi}$ Water	Ref.
1	$B_{dry}\sqrt{\psi} = \dfrac{0.3096}{\sqrt{1 + 0.69/c_\rho}}$	0.3094	0.3095	Dhir & Catton (1982)
2	$B_{dry}\sqrt{\psi}$ depends on ψ	curve $B_{max}\sqrt{\psi}$ Fig. 19a	curve $B_{max}\sqrt{\psi}$ Fig. 19b	This work, $\lambda = 2$
3	$B_{dry}\sqrt{\psi} = \left(\dfrac{1}{1/(c_\rho k_{rw}) + 1/k_{ro}}\right)^{0.5}_{max}$	λ: 0.6935 ∞; 0.6576 2; 0.6063 1; 0.5593 ⅔	λ: 0.7457 ∞; 0.7083 2; 0.6545 1; 0.6052 ⅔; 0.5902 0.6	This work, turbulent term only
4	$B_{dry}\sqrt{\psi} = \dfrac{5}{6}\dfrac{(1 + 5.76\,\psi)^{0.5} - 1}{2C\sqrt{\psi}}$, $C = 0.0157(\Delta\rho/\sigma d_p)^{1/3}$	$(CB_{dry})_{\psi\to 0} = 1.2$; $(CB_{dry}\sqrt{\psi})_{\psi\to\infty} = 1.0$	$= 1.2$; $= 1.0$	Gabor et al. (1981)
5	$B_v\sqrt{\psi} = \dfrac{1}{(1 + c_\rho^{-0.25})^2}$	0.6935	0.7457	Lipinski (1980)
6	$B_v\sqrt{\psi} = \dfrac{0.4524}{(1 + c_\rho^{-0.25})^2}$	0.315	0.3373	Squarer (1981)
7	$B_v\sqrt{\psi} = \dfrac{0.3241}{(1 + c_\rho^{-0.25})^2}\sqrt{\dfrac{\rho_w}{\Delta\rho}}$	0.2249	0.2418	Ostensen & Lipinski (1981)

Jokobsson (1987) for volume heating fall above the curve of porosity 0.4 when $\psi < 10$, that is $B_v > B_{dry}$ in this region. However, this trend is not observed in the case of Freon-113. For methanol, as shown by Figure 21a, the data of Jones et al. (1984) for the bottom-heating case show relatively wide spreading. The data of Tsai and Catton (1983) and Catton and Jokobsson (1987) their data points fall below the curve of porosity 0.4, when $\psi > 10$, in contrast of Barleon and Werle (1981) which, for water and Freon-113, fall above the curve of porosity 0.4 when $\psi > 1{,}000$. The effects of the thermal properties of the particles on these figures are not clear so far.

The prediction equations of various investigators were plotted in Figures 21a, 21b, and 21c for comparison. In Figure 21b, for water, the equation of Gabor et al. (1981) for bottom heating shows that in the region of small particle diameters, their equation comes close to the curve with $\lambda = 0.6$, but the difference increases as $\psi \to 0$. In the region of large particle diameter, their equation predicts a straight line of slope ⅚. When their equations for volumetric and bottom heatings were compared, the ratio, B_v/B_{dry}, is 2 as $\psi \to 0$ and 1.732 as $\psi \to \infty$. Comparisons of this equation with methanol and Freon are also shown in Figures 21a and 21c. The equation of Dhir and Catton (1982) for bottom heating, and the equations of Ostensen and Lipinski (1981), Squarer (1981), and Lipinski (1980), all for volumetric heating, were plotted in these figures. Many experiments were conducted in the transition regions. To be in the high-turbulence region, porous beds with large particles must be used. Therefore, to have the least wall effect, the beds must be of considerable size. Heat loss is also an important factor. Since the dryout heat flux is dependent on particle diameter, porosity, and λ, unless the porous beds used in experiments can be defined rigorously the experimental constants of various prediction equations cannot be the same.

In Figure 22 the effects of λ on the dryout heat flux of beds with large particle diameters are shown. The effect of λ is greater when its value is smaller.

Conclusions

Pool boiling heat transfer from a horizontal surface sinterd with a porous layer has been investigated. A basic dimensionless equation for the flows in a porous matrix was used to analyze one-dimensional pool boiling from porous matrices of different characteristics. Laminar, transition, and turbulent flow regions were investigated. The relationships among the heat flux, dryout heat flux, bed characteristics, Reynolds numbers, and fluid properties were obtained. The case of bottom heating was analyzed. The results were compared with available data of both bottom and volumetric heatings. The following conclusions were obtained.

1. Boiling heat transfer is enhanced by a thin layer of porous matrix sintered on the heater surface. There is an optimum thickness for heat transfer enhancement. As the thickness of the porous layer increases, heat transfer is enhanced in the region of low heat flux but diminished in the region of high heat flux.

2. The maximum critical heat flux of boiling is increased 1.5 times that of a smooth surface by using a sintered porous layer on the heater surface.

3. For heaters with thick porous layers, the following statements apply. The boiling curves show a noticeable change in

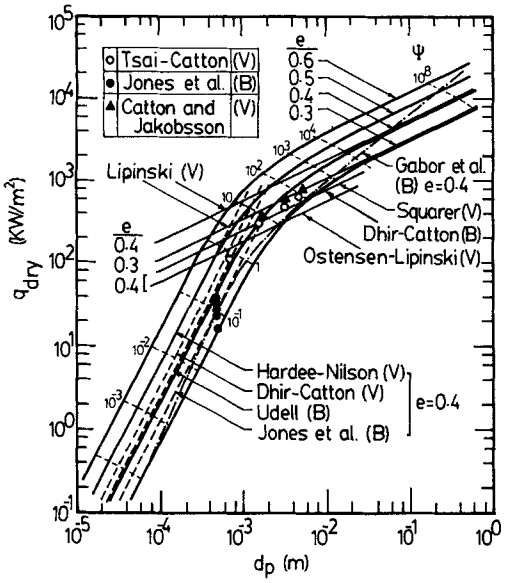

Figure 21a. Dryout heat flux vs. particle diameter at various ψ and porosities, methanol.
Thick porous matrix; $\lambda = 2$

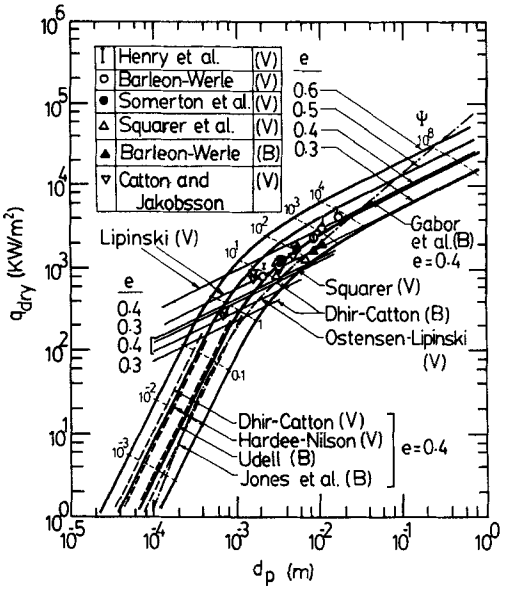

Figure 21b. Dryout heat flux vs. particle diameter at various ψ and porosities, water.
Thick porous matrix; $\lambda = 2$

slope, indicating difficulties in liquid supply to the heater surface. The dimensionless heat fluxes before and at dryout are almost independent of thickness. For a given fluid and saturation temperature, the dimensionless dryout heat flux is dependent on the parameter ψ and the pore size distribution index λ. A uniform pore size structure has the highest dimensionless dryout heat flux. Equations in this analysis show that the slope of log q_{dry} vs. log d_p is 2 in the laminar region and is ½ in the high-turbulence region. Dependence of these lines on porosity can be calculated at various ψ for a given pore size distribution index.

The prediction equations proposed by various investigators for the dryout heat flux can be written in simpler dimensionless

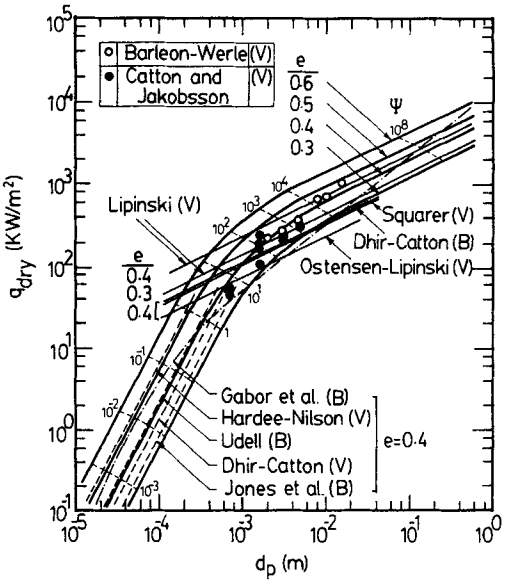

Figure 21c. Dryout heat flux vs. particle diameter at various ψ and porosities, R-113.
Thick porous matrix; $\lambda = 2$

forms. A number of prediction equations are comparable with this analysis by choosing proper values of λ and ψ.

4. For heaters with thin porous layers, the dimensionless dryout heat flux increases with decreasing thickness of the porous layer. For the same thickness, the matrix with larger porosity has higher dryout heat flux. For the same porosity, a matrix with larger particle diameter has a higher dryout heat flux.

5. The Reynolds numbers of the vapor and liquid flows are related to the dimensionless heat flux B and the parameter ψ. Most experimental data fall in the region where $Re_{1,v} < 1{,}000$. For water, the flow changes from laminar to transition flow at $\psi \simeq 0.1$, and from transition to highly turbulent flow at $\psi \simeq 10{,}000$.

6. The porous layers used in experimental work are rarely described rigorously. Size distribution is often unknown or not given. This information is important for interpreting the experimental results.

Acknowledgment

This work was sponsored by the National Science Council, R.O.C. under Grant No. NSC74-0402-E002-11.

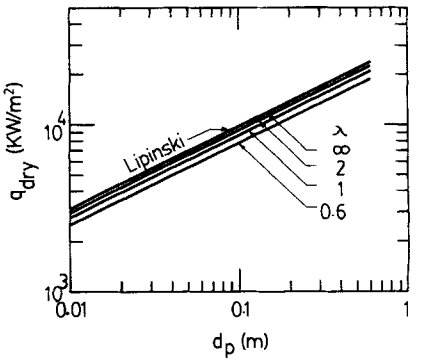

Figure 22. Effect of pore size distribution index on dryout heat flux vs. particle diameter, water.
Thick porous matrix; porosity 0.4, $\psi \to \infty$

Notation

a, b, c = coefficients, Eq. 14a, = 1.417, 2.120, 1.263
B = dimensionless heat flux, $= q\nu_v/h_{fg}k\,\Delta\rho g$
B_{dry} = dimensionless dryout heat flux, $= q_{dry}\nu_v/h_{fg}k\,\Delta\rho g$
B_{max} = maximum dimensionless heat flux B for infinitely thick porous layer
c_ν = ratio of kinematic viscosity of liquid to vapor
c_ρ = ratio of density of liquid to vapor
d'_m = equivalent diameter of the pore channel, m
d_p = particle diameter, m
D = effective diameter of tube or duct, m
e = porosity
g = gravitational acceleration, 9.8 m/s^2
h_{fg} = heat of vaporization, kJ/kg
k = permeability, m^2
k_{rv} = relative permeability of vapor
k_{rw} = relative permeability of liquid
L = thickness of porous layer, m
L_d = dimensionless thickness of porous layer, $\Delta\rho\, gL/(\sigma/\sqrt{k/e})$
p_c = capillary pressure, N/m^2
p_{cd} = dimensionless capillary pressure, $p_c/\Delta\rho\, gL$
Δp = pressure drop over L, N/m^2
q = heat flux, kW/m^2
q_{dry} = dryout heat flux, kW/m^2
$Re_{1,v}$ = vapor Reynolds number, Eq. 18
$Re_{1,w}$ = liquid Reynolds number, Eq. 20
s = specific surface area, $= 6/d_p$ for sphere, m^2/m^3
S = absolute liquid saturation
Se = relative liquid saturation, $= (S - S_r)/(S_m - S_r)$
S_m = maximum liquid saturation
S_r = residual liquid saturation
u = superficial velocity, m/s
u_1 = true velocity, $= u/e$, m/s
y = distance from heater surface, m
y_d = dimensionless distance from heater surface, y/L

Greek letters

$\beta = 1.75d_p/[150(1 - e)]$
λ = index of pore size distribution
μ = viscosity, kg/m · s
ν = kinematic viscosity, m^2/s
ρ = density, kg/m^3
σ = surface tension, N/m
τ_w = shear stress at wall, N/m^2
ϕ = friction factor
ψ = dimensionless parameter, Eq. 9c

Subscripts

v = vapor phase
w = liquid phase

Literature Cited

Afgan, N. H., L. A. Jovic, S. A. Kovalev, and V. A. Lenykov, "Boiling Heat Transfer from Surfaces with Porous Layers," *Int. J. Heat Mass Trans.*, **28**(2), 415 (1985).

Barleon, L., and H. Werle, KfK-3138, Kernforschungszentrum Karlsruhe (1981).

Bau, H. H., and K. E. Torrance, "Boiling in Low-permeability Porous Materials," *Int. J. Heat Mass Trans.*, **25**(1), 45 (1982).

Brooks, R. H., and A. T. Corey, "Properties of Porous Media Affecting Fluid Flow," *J. Irrig. Drainage Div., Proc. ASCE*, **IR2**, 4855 (June, 1966).

Catton, I., and J. D. Jakobsson, "The Effect of Pressure on Dryout Heat Flux of a Saturated Bed of Heat-Generating Particles," *J. Heat Trans.*, **109**, 185 (Feb., 1987).

Chang, S. H., and S. H. Kim, "Derivation of a Dryout Model in a Particle Debris Bed with the Drift Flux Approach," *Nuc. Sci. Eng.*, **91**, 404, Table IV (1985).

Corey, A. T., *Mechanics of Heterogeneous Fluids in Porous Media*, Water Resources pub. (1977).

Cornwell, K., B. G. Nair, and T. D. Patten, "Observation of Boiling in Porous Media," *Int. J. Heat Mass Trans.*, **19**, 236 (1976).

Coulson, J. M., and J. F. Richardson, *Chemical Engineering*, Pergamon Press, v. 2, 129–132, (1978).

Czikk, A. M., P. S. O'Neill, and C. F. Gottzmann, "Nucleate Boiling from Porous Metal Films: Effect of Primary Variables," *Adv. Enhanced Heat Trans.*, **HTD-18**, 109 (1981).

Dhir, V. K., and I. Catton, "Boiling in a Porous Bed," *Appl. Sci. Res.*, **38**, 69 (1982).

Ferrell, J. K., and J. Alleavitch, "Vaporization Heat Transfer in Capillary Wick-Structures," *Chem. Eng. Prog. Symp. Ser.*, Heat Transfer—Minneapolis, **66**(102), 82 (1970).

Gabor, J. D., J. C. Cassulo, S. W. Jones, and D. R. Pedersen, "Studies of Heat Removal from Fuel Debris," *Trans. ANS*, **39**, 642 (1981).

Hardee, H. C., and R. H. Nilson, "Natural Convection in Porous Media with Heat Generation," *Nuc. Sci. Eng.*, **63**, 119 (1977).

Ito, T., K. Nishikawa, and K. Tanaka, "Evaluation of Potentially High Performance Porous Surfaces," *Refrigeration*, **57**(651), 25 (Jan., 1982).

Jones, S. W., E. Epstein, S. G. Bankoff, and D. R. Pedersen, "Dryout Heat Fluxes in Particulate Beds Heated through the Base," *J. Heat Trans.*, **106**, 176 (Feb., 1984).

Lipinski, R. J., "A Particle-bed Dryout Model with Upward and Downward Boiling," *Trans. ANS*, **35**, 358 (1980).

———, "A One-dimensional Particle-Bed Dryout Model," *Trans. ANS*, **38**, 386 (1981).

Milton, R. M., and C. F. Gottzmann, "High-efficiency Hydrocarbon Reboilers and Condensers," AIChE 71st Nat. Meet., Dallas (Feb. 21, 1972).

Ostensen, R. W., and R. J. Lipinski, "A Particle-bed Dryout Model Based on Flooding," *Nuc. Sci. Eng.*, **79**, 110 (1981).

Squarer, R. D., "The Limiting Dryout Heat Flux in a Large-Particle Heat Generating Debris Bed," *Trans. ANS*, **39**, 1049 (1981).

Tsai, F. P., and I. Catton, "On Dryout Heat Flux and Pressure Drop of a Submerged Inductively Heated Bed Flow from Below," *AIChE Symp. Ser.*, Heat Transfer, **79**(225), 296, (1983).

Udell, K. S., "Heat Transfer in Porous Media Considering Phase Change and Capillarity—The Heat Pipe Effect," *Int. J. Heat Mass Trans.*, **28**(2), 485 (1985).

Manuscript received in two parts, Nov. 5, 1986 and Dec. 4, 1986, and revision received May 13, 1987.